

Cholesterol Modulates the Membrane Effects and Spatial Organization of Membrane-Penetrating Ligands for G-Protein Coupled Receptors

George Khelashvili,* Sayan Mondal, Olaf S. Andersen, and Harel Weinstein

Department of Physiology and Biophysics, Weill Cornell Medical College of Cornell University, New York, New York

Received: July 9, 2010; Revised Manuscript Received: August 10, 2010

The ligands of certain G-protein coupled receptors (GPCRs) are membrane soluble and reach their target from the lipid bilayer. Lipid composition and dynamics will therefore modulate the activity of these receptors, but specific roles of lipid components, including the ubiquitous cholesterol (Chol), are not clear. We have probed the organization and dynamics of such a lipid-bilayer-penetrating ligand, the endogenous ligand for the κ -opioid receptor (KOR) dynorphin A (1–17) (DynA), using molecular dynamics (MD) simulations of DynA in cholesterol-depleted and cholesterol-enriched model membranes. DynA is found to penetrate deep inside fluid dimyristoylphosphatidylcholine (DMPC) bilayers, and resides with its N-terminal helix at ~ 6 Å away from the bilayer midplane, in a tilted orientation, at an $\sim 50^\circ$ angle with respect to the membrane normal. In contrast, DynA inside DMPC/Chol membranes with 20% cholesterol (DMPC/Chol) is situated with its helical segment ~ 5 Å higher, i.e., closer to the lipid/water interface and in a relatively vertical orientation. The DMPC membrane shows greater thinning around the insertion and permits a stronger influx of water inside the hydrocarbon core than the DMPC/Chol membranes. Relating these results to data about key GPCR residues that have been implicated in interactions with membrane-inserting GPCR ligands, we conclude that the position of DynA in DMPC/Chol, but not in pure DMPC, correlates with generally proposed GPCR ligand entry pathways. Our predictions provide a possible mechanistic explanation as to why DynA binding to KOR, and the subsequent activation of the receptor, is facilitated in cholesterol-enriched environments. A quantitative description of DynA-induced membrane deformations is obtained with a continuum theory of membrane deformations (CTMD) that is based on hydrophobic matching. Comparison with the MD data reveals the significance of the lipid tail packing energy contribution in the DMPC/Chol mixtures in predicting equilibrium membrane shape around DynA. On this basis, specific corrections are introduced to this energy term within the CTMD framework, thereby extending the applicability of the CTMD framework to lipid raft mixtures and their interactions with GPCR proteins and their ligands.

Introduction

Members of the large and diverse G-protein coupled receptor (GPCR) family of transmembrane (TM) proteins modulate cellular responses to a large variety of physical or chemical stimuli.^{3–9} In their activated form, these receptors interact with G protein partners, to trigger events that ultimately lead to a signaling cascade.⁴ Compelling evidence suggests that rafts, specialized plasma membrane domains that are enriched in cholesterol and saturated lipids,^{1,2,10–12} play a role in the signaling and trafficking of GPCRs. A mechanistic understanding about the interplay between these lipid membrane micro-domains and GPCR function is lacking.^{1,2}

Experimental information about the possible relation between GPCR function and raft structure and dynamics comes from biochemical and biophysical studies conducted *in vitro* on cell membranes and model lipid assemblies.^{1,2,12} These studies usually rely on the observation that, due to their liquid-ordered (L_o) properties, rafts present a more rigid environment compared to other membrane compartments and therefore are resistant to low-temperature solubilization by various detergents, such as Triton X-100.^{13–21} Thus, treatment of cell plasma membranes

with detergent allows for the isolation of rafts and has provided clues on putative raft components, most notably glycosylphosphatidylinositol (GPI)-anchored proteins^{22,23} and various TM proteins, such as GPCRs.^{1,2} In addition, comparison of the activities of various GPCRs in cholesterol-depleted vs intact cell membranes has related functional efficacies of some GPCRs to lipid rafts. The main conclusion that emerged from these studies is that some GPCRs, such as the κ -opioid receptor (KOR),²⁴ function better in cholesterol-enriched environments, whereas others (e.g., rhodopsin²⁵) require relatively low-cholesterol, liquid-disordered membrane platforms for effective function.

The participation of lipid rafts in the regulation of GPCR function has been linked to cholesterol's ability to affect functionally important modes of motion in GPCRs,^{3,9,26} through direct cholesterol–protein interactions or indirectly,^{10,11} by altering the biophysical properties of the lipid bilayer, and possibly by a combination of these effects. For example, from a microsecond-long molecular dynamics (MD) trajectory of rhodopsin in a mixed cholesterol-containing lipid environment, we concluded that the cholesterol dynamics around GPCR evince a direct relation to structural changes associated with GPCR activation, that are triggered by local perturbations and propagated into larger-scale TM movements.²⁷

* Corresponding author. Mailing address: Department of Physiology and Biophysics, Weill Medical College of Cornell University, 1300 York Avenue, room LC-501B, New York, NY, 10021. E-mail: gek2009@med.cornell.edu. Phone: 212-746-6539. Fax: 212-746-6226.

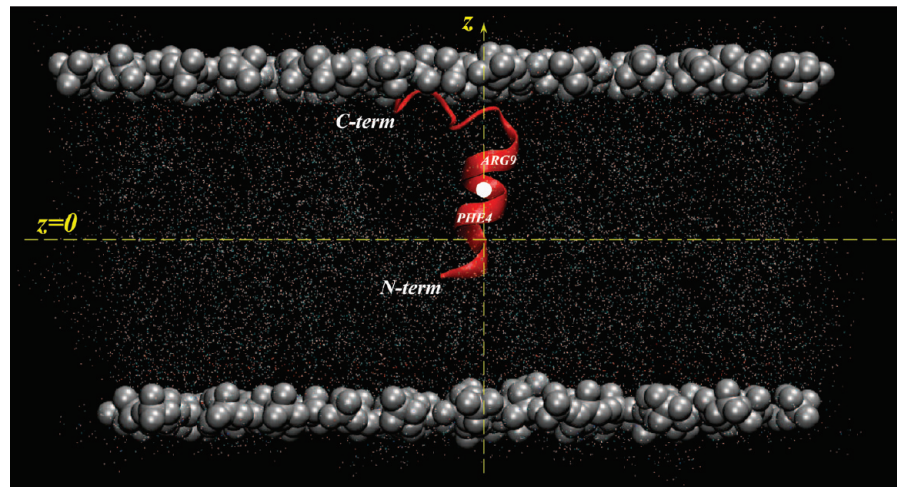


Figure 1. Snapshot of the starting configuration of the DMPC/Chol system 3 (see Table 1). The DynA peptide is shown in red, and the membrane interior is depicted by a density of dots bounded by the space-filling representation of PO_4 groups of the DMPC. Water and salt are removed for clarity. Vertical and horizontal dashed lines represent the bilayer normal z axis and the location of the $z = 0$ bilayer midplane, respectively. The center of mass of the 4–9 helix (white circle) and the positions of residues Phe4 and Arg9 are indicated on the DynA structure.

Although these simulations provided a possible mechanistic explanation for the observation that rhodopsin function is optimized in membranes with low Chol content,²⁵ at least two other poorly understood phenomena hinder progress toward adequate consideration of lipid rafts in GPCR signaling. One relates to the finding that GPCRs move in and out of rafts in response to agonist ligand binding;^{1,2} the other pertains to the finding that certain GPCR ligands reach their target binding sites from the lipid bilayer, rather than through direct partitioning from the aqueous solution into the GPCR. Well-established examples of such ligands include dynorphin A^{1–17} (DynA),^{28,29} which is an endogenous ligand for KOR, and the cannabinoid CB2 receptor ligand AM841.^{30,31} Furthermore, 11-cis-retinal may enter opsin from the lipid bilayer.³²

It is reasonable to suspect that the local lipid composition of the cell membrane will modulate not only the local concentrations of these bilayer-embedded ligands but also their organization inside the lipid bilayer, which impacts the mode of ligand–GPCR interaction. For example, we have recently predicted that the orientational freedom of bilayer-inserting TM domains in cholesterol-enriched membrane domains will be influenced by the aligning field induced by cholesterol, which would enforce an orientational preference for the insertions along the membrane normal.³³ Moreover, a higher concentration of cholesterol could reduce the membrane partitioning of the ligands, due to cholesterol's condensing effect.^{33–38}

To address the need for this type of information concerning GPCRs that are activated by membrane-embedded ligands, we have probed the effects of cholesterol on the organization and dynamics of lipid-bilayer-bound GPCR ligands. From MD simulations of DynA in model membranes, we show that DynA can penetrate deep inside liquid-disordered dimyristoylphosphatidylcholine (DMPC) bilayers, to reside with its N-terminal helix (Figure 1) at $\sim 6 \text{ \AA}$ away from the bilayer midplane. Furthermore, DynA in DMPC membranes assumes a tilted orientation, up to an angle of $\sim 50^\circ$ with respect to the membrane normal, in agreement with previous MD studies of DynA in the same lipid bilayers.^{39,40} We contrast these results to those obtained for DynA in membranes composed of a mixture of DMPC containing 20% cholesterol (DMPC/Chol), a mixture that shows raft-like liquid-order properties.^{33–35} In these membranes, we find DynA to be located so that its helical segment is $\sim 5 \text{ \AA}$ higher, i.e., toward the lipid/water interface compared

TABLE 1: Summary of Simulated Systems^a

	DMPC/Chol 1, DMPC/Chol 2, DMPC/Chol 3, DMPC, 0%	20% 1	20% 2	20% 3
temperature, $^\circ\text{C}$	35	35	35	35
$N_{\text{DMPC}}^{\text{upper}}$	94	74	74	75
$N_{\text{DMPC}}^{\text{lower}}$	98	80	80	80
$N_{\text{CHOL}}^{\text{upper}}$	0	19	19	19
$N_{\text{CHOL}}^{\text{lower}}$	0	20	20	20
N_{water}	11185	9870	9879	9902
N_{K}	25	22	22	23
N_{Cl}	29	26	26	27
$Z_{\text{DynA}}, \text{\AA}$	7	7	7	6.5
β_{DynA}	35°	35°	35°	11°

^a The table shows the number of DMPC and cholesterol molecules in the upper leaflets (where DynA resides) and the lower leaflets, as well as the number of water molecules, salt ions, initial z coordinate for the DynA center of mass, and the starting DynA tilt angles. Note that, although the starting DynA tilt angles in the DMPC/Chol 1 and DMPC/Chol 2 systems are similar, the initial membrane configuration around the peptide in these simulations is different.

to pure DMPC, and in a relatively vertical orientation. Furthermore, the pure DMPC membrane shows more thinning around the inserted DynA and a higher concentration of water in the hydrocarbon core in the vicinity of the peptide.

These results are considered in the context of experimental findings and theoretical predictions suggesting that membrane-embedded ligands interact with their target GPCRs via specific pathways, such as through openings around receptor extracellular ends of TM6/TM7,^{30,31} TM5/TM6,^{32,45} or TM7/TM1.³² Our findings suggest how the type of conditions achieved in lipid rafts may modulate interactions of bilayer-penetrating ligands with their partner GPCRs. Specifically, our results provide a mechanistic explanation for how DynA binding to the κ -opioid receptor can be facilitated in cholesterol-enriched environments.²⁴

To extend the mechanistic insights obtained from the MD simulations, we proceeded to quantify the energies involved in the DynA-induced membrane deformations. To this end, we evaluated the performance of the continuum theory of membrane deformations (CTMD), based on hydrophobic matching,^{41–44} in comparison to the MD results. The detailed comparative analysis revealed the importance of the lipid tail packing energy contribution in liquid-ordered DMPC/Chol mixtures for the

quantitative prediction of the equilibrium membrane shape around DynA. On this basis, we developed the necessary correction for this energy term within the CTMD framework, which leads to ways of extending the applicability of the efficient CTMD framework to lipid raft mixtures and their interactions with GPCR proteins and their ligands.

Methods

Membrane Systems Studied. Molecular dynamics (MD) simulations of dynorphin A^{1–17} (YGGFLRIRPKLKWDNQ) (DynA) immersed in bilayers consisting of either DMPC or DMPC plus 20% cholesterol (DMPC/Chol) were conducted at 35 °C. These particular membrane compositions were chosen on the basis of several considerations: By simulating these membranes at a temperature of 35 °C, we expect to explore the organization and dynamics of DynA in membranes with different fluidity properties, according to the previously proposed temperature–composition diagram for DMPC/cholesterol bilayers.⁴⁸ In particular, (i) DMPC is commonly used in physicochemical studies because of its relatively low gel-to-fluid transition temperature;⁴⁸ (ii) pure DMPC is in a liquid-disordered state, whereas a mixture of DMPC plus 20% cholesterol is expected to have characteristics of a raft-like liquid-ordered state; (iii) DMPC/cholesterol systems have been widely studied both experimentally and computationally, and have been used previously for studies of DynA and other membrane penetrating peptides.^{39,40,46,47} Such results are useful for comparisons and validation.

The initial configuration of DynA peptide was the same structure utilized earlier,^{39,40} which was derived from NMR studies of DynA in dodecylphosphocholine (DPC) micelles.⁴⁹ In this structure, the residue stretch 3–9 of the N-terminal region of DynA is α -helical (see Figure 1). As in previous studies,^{39,40} although residues 1 and 2 were not part of the α -helix in the NMR structure, the N-terminal helical region was extended in the initial configuration to include these two residues.

We carried out one simulation with DMPC and three separate simulations with DMPC plus 20% Chol, in which we varied the DynA starting orientation inside the membrane and the initial lipid distribution around DynA. The initial conditions in all these systems are summarized in Table 1, and Figure 1 illustrates the starting configuration of DynA in one of the DMPC/Chol mixtures. The orientation of DynA (β_{DynA} in Table 1) was assessed throughout by monitoring the angle between the peptide segment connecting residues 4–9 and the bilayer normal z axis; the position of DynA inside the membrane (Z_{DynA} in Table 1) was evaluated by tracking the vertical distance between the center of mass of the DynA 4–9 segment and the bilayer midplane.

Building and Simulating Model Membranes. The peptide–bilayer complexes (see Table 1) were built with the CHARMM-GUI Membrane Builder web tool,⁵⁰ using the CHARMM27 force field for DynA,⁵¹ and refined CHARMM parameters for saturated lipid chains,⁵² polyunsaturated lipid chains,⁵³ and cholesterol.⁵⁴ Briefly, the macromolecule/membrane complex-building process in CHARMM-GUI consists of several steps:⁵⁰ (1) the Membrane Builder is first fed the initial structure of the DynA peptide; (2) the membrane normal axis z is defined such that $z = 0$ is at the center of the bilayer, and the peptide is placed in the desired orientation and position with respect to the z axis and the $z = 0$ plane, respectively; (3) the system size is chosen by picking the desired lipid species, providing the desired number of lipids on two leaflets, and specifying the number of water molecules to be included per lipid headgroup.

Because DynA has been chosen to be initially situated mostly in one leaflet (Figure 1), the resulting membrane patches were asymmetric (see Table 1), to keep the starting area of the two leaflets approximately the same; (4) after adding salt ions for charge neutrality, each component is then built and assembled. CHARMM-GUI utilizes a structural library containing 2000 different conformations for each lipid molecule, so that, with different initial random seed numbers, the Builder generates a different lipid bilayer conformation. Care was also taken to resolve bad protein/lipid and lipid/lipid contacts, which was achieved using the replacement method. The final assembled structures were additionally checked for any remaining bad contacts, such as between the cholesterol ring and other types of lipids or protein.⁵⁰

After 5400-step initial energy minimization, all the systems were simulated for 150 ns (including 70 ns of equilibration) using the NAMD modeling package⁵⁵ and the CHARMM27 force field.^{51–54} The simulations were conducted under constant temperature and pressure conditions with anisotropic pressure coupling and utilizing PME for long-range electrostatics.⁵⁶ The Nose–Hoover Langevin piston method^{57,58} was used to control the target pressure with the LangevinPistonPeriod set to 100 fs and LangevinPistonDecay set to 50 fs. All MD simulations were performed with rigidBonds allowing 2 fs time step.

Analysis of DynA Helix Parameters. To quantify changes in the DynA structure and dynamics, such as peptide helicity and tilt throughout the MD trajectories, we used the Trajelix tool of the publicly available software Simulaid.⁵⁹ Briefly, Trajelix evaluates the integrity of a helix by performing DSSP (define secondary structure of proteins) checks,⁶⁰ and the tilt angle of a helix with respect to a laboratory frame coordinate axis is defined as the angle between the helical axis and the lab axis.

Figure 2 shows the helicity of the DynA peptide in the simulated membranes and reveals that, overall, the helical structure of the DynA 4–9 segment is better stabilized in the cholesterol-containing membranes. In the DMPC bilayer, the 4–9 segment is relatively frayed. This region is also somewhat distorted in DMPC/Chol simulation 3, as compared to the two DMPC/Chol simulations. Accordingly, for calculations of the DynA tilt (see Results and Discussion), we used in all the systems only those trajectory frames where the entire 4–9 segment was helical.

Quantitative Description of DynA-Induced Membrane Deformations. To quantify the DynA-induced membrane deformations observed in the simulated systems, we applied the continuum theory of membrane deformations (CTMD) based on hydrophobic matching.^{41–44} In the CTMD approach, a mismatch between the thickness of the hydrophobic core of an unperturbed bilayer, d_0 , and the length, l , of the hydrophobic exterior surface of a bilayer inclusion causes a deformation of the bilayer around the insertion. The CTMD is based on the assumption that the hydrophobic interactions between a TM and the bilayer are strong enough to ensure that there is no exposure of hydrophobic residues to water, resulting in a membrane thickness of $d_0 - l$ at the inclusion/bilayer boundary.^{42,43} In the CTMD, the free energy functional describing bilayer deformations, ΔG_{def} , is treated on the continuum level, and contains contributions due to changes in bilayer thickness and in monolayer curvature, as well as due to surface tension:^{42,43,61}

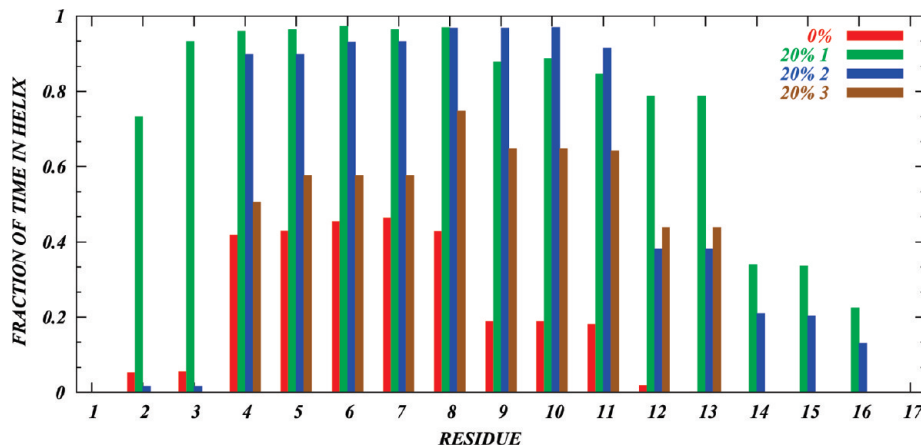


Figure 2. Helicity of the DynA peptide in the model membranes. The fraction of time each residue of DynA spends in a helix is plotted for all simulated systems. For this analysis, only converged trajectories (after 70 ns) were used.

$$\Delta G_{\text{def}} = \int_{\Omega} \frac{1}{2} \left(K_a \left(\frac{u}{d_0} \right)^2 + K_c \left(\frac{\partial^2 u}{\partial x^2} + \frac{\partial^2 u}{\partial y^2} - c_0 \right)^2 + \alpha \left[\left(\frac{\partial u}{\partial x} \right)^2 + \left(\frac{\partial u}{\partial y} \right)^2 \right] \right) \quad (1)$$

In the above, K_a and K_c are the compression-expansion and bending moduli, respectively, α is the surface tension, u represents local perturbations in monolayer thickness (which may differ in the two leaflets), and c_0 denotes monolayer spontaneous curvature. Following the works of Andelman et al.⁶² and Khelashvili et al.,⁶³ we represent c_0 as the weighted sum of the spontaneous curvatures of the pure lipid constituents: $c_0 = c_0^{\text{DMPC}} \phi^{\text{DMPC}} + c_0^{\text{CHOL}} \phi^{\text{CHOL}}$, where c_0^{DMPC} and c_0^{CHOL} are the spontaneous curvatures and ϕ^{DMPC} and ϕ^{CHOL} are mole fractions of DMPC and cholesterol, respectively. We approximate $c_0^{\text{DMPC}} = 0$, due to the mostly cylindrical shape of the (saturated) DMPC lipid,⁶⁴ and used $c_0^{\text{CHOL}} = -1/25 \text{ \AA}^{-1}$.⁶⁵

The CTMD algorithm assumes a symmetric deformation and searches for the equilibrium membrane shape around a TM inclusion by minimizing G_{def} subject to boundary conditions in the bulk, and at the insertion/bilayer interface. In particular, far from the inclusion, the bilayer “shape” is that of an unperturbed bilayer.^{42,43} At the inclusion surface, the monolayer deformation u_0 is given by the mismatch $(d_0 - l)/2$. Lastly, the boundary condition for the slope of the deformations at the inclusion interface accounts for lipid packing adjacent to the insertions: $(\partial u / \partial r)_{r_0} = s$, where r_0 is the radius of TM insertion and s is the so-called packing parameter.^{42–44} In geometric terms, the packing parameter is given by $\tan \theta$, where θ represents the angle between the slope of the deformation and the membrane horizontal plane.

In order to obtain the steady state membrane deformations, the CTMD algorithm performs a *self-consistent* minimization in which the packing parameter value is varied, and for each s , the shape profile $u(x, y)$ that minimizes G_{def} is obtained from eq 1. The G_{def} vs s relationship identifies a value of the packing parameter s_{min} that minimizes the free energy functional, and the final equilibrium shape is the one that corresponds to this s_{min} .^{42,43}

To describe DynA-induced membrane deformations in DMPC and DMPC/Chol membranes with the CTMD approach, we assumed that for each simulated system the hydrophobic thickness of bilayer at the inserted DynA is the lipid phospholipid head-to-head distance, $d_{\text{HH}}^{\text{TM}}$, as measured from our MD simulations (see the Results and Discussion, Figure 6), whereas

TABLE 2: Values for Different Constants in eq 1 Used in the Minimization Procedure

	DMPC	DMPC/Chol	references
K_a (N/Å)	1.44×10^{-11}	6×10^{-11}	102
K_c (N × Å)	5.6×10^{-10}	16.8×10^{-10}	34, 103
α (N/Å)	3×10^{-13}	3×10^{-13}	42, 101

the thickness of the unperturbed bilayer $d_{\text{HH}}^{\text{bulk}}$ is that measured at the edges of the simulation box. Therefore, we imposed the boundary condition that the monolayer deformation u_0 at the inclusion surface is given by $(d_{\text{HH}}^{\text{bulk}} - d_{\text{HH}}^{\text{TM}})/2$. Treating membrane deformations around DynA as azimuthally isotropic, we then solved eq 1 for different values of the s parameter following the procedure in refs 42–44, to obtain s_{min} and consequently $u(x, y) \equiv u(r)$ that minimized the free energy functional. In the process, we utilized a set of material constants for DMPC and DMPC/Chol obtained from experimental measurements (see Table 2).

Calculation of Cholesterol Tilt Modulus. We have previously described the procedure for calculating the cholesterol tilt modulus χ from MD simulations.³³ Briefly, the normalized probability density $P(\theta)$ of the cholesterol tilt angle with respect to the bilayer normal is constructed for each simulated system. The tilt angle, θ , is defined as the polar angle between the vector C3–C17, commonly used to describe the cholesterol ring plane orientation and the bilayer normal. As usual for polar coordinates, θ is defined in the range [0°; 180°]. In this definition, $\theta = 0$ represents a cholesterol orientation where the ring plane is parallel to the bilayer normal z axis. The $P(\theta)$ distribution is obtained by creating a cholesterol orientational angle histogram in the angular range $\theta \subset [0^\circ; 90^\circ]$. To calculate the cholesterol tilt modulus, a quadratic fit is performed for the $-k_B T \log[P(\theta) / \sin \theta]$ function in the [8°; 20°] interval, a range chosen to represent the best-sampled angular region and at the same time to limit the fit to low θ regime.^{33,66} Finally, χ is directly measured from the coefficient that corresponds to the best fit.

Results and Discussion

Equilibration of the Model Membranes and Dynamics of DynA Peptide. The convergence of the simulated systems was monitored through the evolution of several key structural properties of the bilayers, as well as by tracking the dynamics of the DynA peptide inside. The simulation box dimensions were constant within fluctuation profiles for the latter half of the 150 ns trajectories for all the membranes (data not shown), and equilibrium values for the areas per lipid headgroup for DMPC

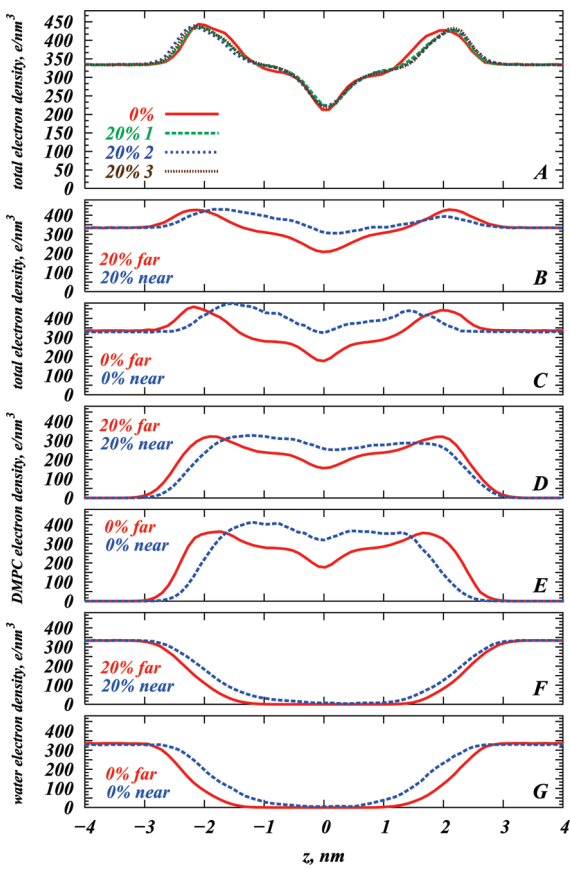


Figure 3. (A) Overall electron density profiles (excluding DynA) for all the simulated membranes. (B) DMPC/Chol systems (averaged over the three simulations) calculated separately inside a 20 Å radial shell around the inserted DynA (near) and beyond this zone (far). (C) Pure DMPC system. (D) DMPC electron density profiles in the DMPC/Chol systems. (E) DMPC electron density profiles in pure DMPC. (F) Water electron density profiles in the DMPC/Chol systems (averaged over the three simulations). (G) Water electron density profiles in the pure DMPC system. The electron densities were constructed by dividing the simulation cell into slabs in the z direction, and by counting the number of electrons corresponding to the atoms in each slab. The analysis was carried out only on the converged equilibrated trajectories, after 70 ns of simulations.

and DMPC/Chol membranes, calculated by dividing the area of the simulation box by the number of DMPC+Chol molecules per leaflet, were 53 ± 2 and 44 ± 2 Å², respectively (the three DMPC/Chol simulations gave similar results).

Although DynA has an effect on the organization of the bilayers (see below), the observed lateral compression of the DMPC/Chol membranes is consistent with the well-known condensing effect of cholesterol on phospholipids,^{33–38} and is generally accompanied by a concomitant increase in bilayer thickness.^{33–38,67–70} Thus, the change in peak-to-peak distance on the electron density plots in Figure 3A shows that Chol addition increases the average distance, d_{HH} , between the DMPC phosphate atoms in the opposing leaflets by ~5 Å. This value is close to previous reports.^{38,67,71,72} We also find d_{HH} to be strongly dependent on the radial distance from DynA. In particular, as evidenced from Figure 3B–E, in all the systems, d_{HH} measured inside a 20 Å radial shell around the inserted DynA is smaller compared to that calculated outside this DynA-neighboring region. Thus, membranes in all the studied systems show apparent thinning around the insertion (see below). To relate these bilayer deformations to the dynamics of DynA inside membranes, we proceed with a description of DynA organization

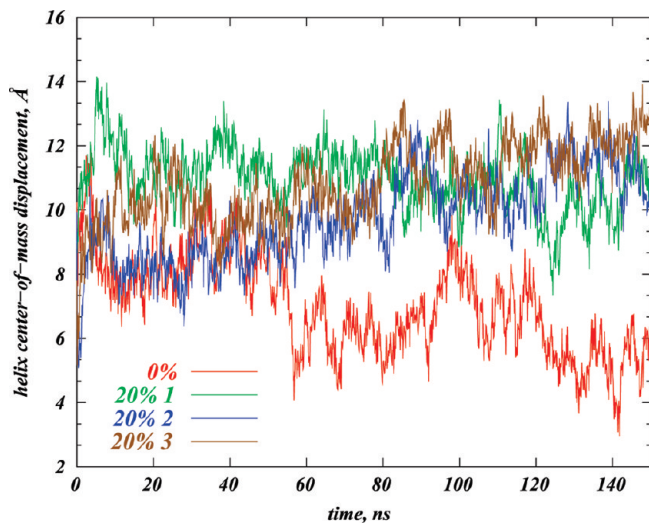


Figure 4. DynA dynamics in the model membranes. Evolution of the vertical displacement from the bilayer midplane of the DynA 4–9 segment center of mass in all simulated systems.

in the model bilayers and then discuss the response of DMPC and DMPC/Chol membranes to DynA insertion.

Figure 4 shows the time evolution of the vertical position Z_{DynA} measured from the membrane midplane, showing that DynA organization is substantially different in DMPC and DMPC/Chol. Z_{DynA} in DMPC is 6 ± 1 Å, a value consistent with earlier simulations on the same systems,^{39,40} whereas in all three DMPC/Chol bilayers DynA Z_{DynA} moves outward, to $Z_{\text{DynA}} = 11 \pm 1$ Å. Thus, in cholesterol-enriched membranes, DynA is situated with its 4–9 helical segment ~5 Å “higher”, i.e., toward the lipid–water interface, compared to the pure DMPC system.

In the pure DMPC membrane, DynA is positioned deeper than in the Chol-containing membrane due to the absence of the aligning field produced by Chol³³ that would also keep the peptide in a relatively straight orientation (aligned with the z axis). Thus, DynA also assumes a more tilted orientation in pure DMPC. This is because lipid acyl chains generally show lower order toward their terminal methylene groups compared to those close to the lipid backbone region (see below and Figure 7). Hence, when DynA is localized closer toward the interface, it can be expected to have limited flexibility compared to DynA that is positioned “lower”, in the hydrocarbon core (see below). DynA is therefore more upright in DMPC/Chol than in DMPC bilayers; we calculate the angle between the DynA 4–9 segment and the bilayer normal β_{DynA} to be ~50° for DMPC, in good agreement with previous MD studies of DynA in DMPC membranes,^{39,40} and ~32 ± 8° for DMPC/Chol (error bars represent standard deviation from the three DMPC/Chol simulations). This is evident in Figure 5, which shows the final snapshots, after 150 ns, of DynA immersed into DMPC and DMPC/Chol (20% 1) membranes. Moreover, Figure 5 not only suggests a different DynA organization in these bilayers but also highlights the different responses of Chol-free and Chol-enriched membranes to DynA insertion. In particular, the pure DMPC membrane appears to be substantially deformed around the insertion, whereas the DMPC/Chol bilayer shows a smaller deformation. This point is addressed more quantitatively below.

DynA Dynamics in DMPC/Cholesterol Membranes Results in Bilayer Thinning and Water Penetration. Figure 6 shows the membrane thickness, d_{HH} , as a function of radial distance from DynA. The values, normalized relative to those far from the insertion, are plotted for the simulated systems

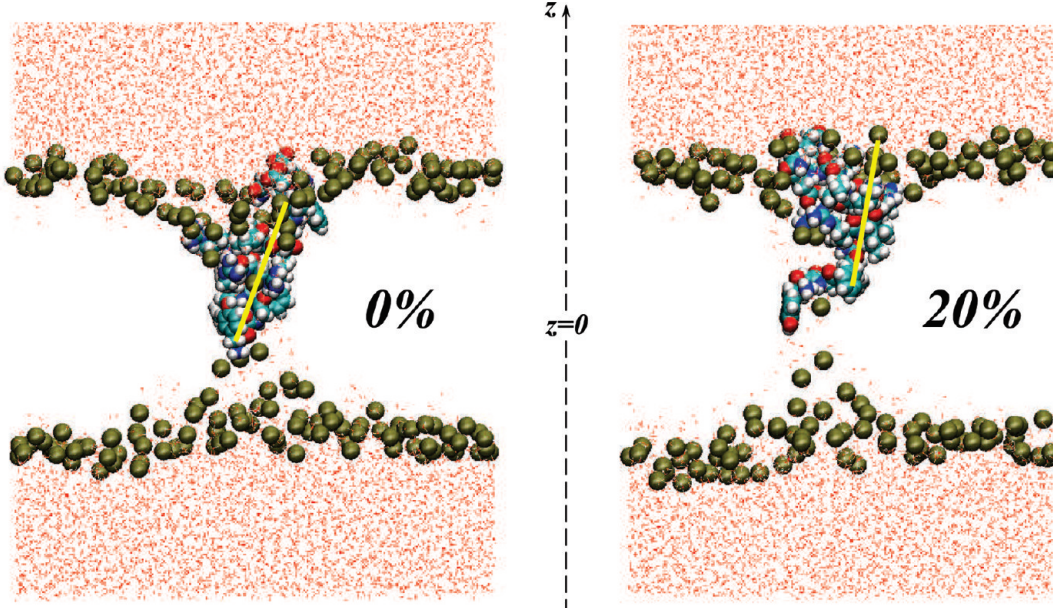


Figure 5. Final snapshots, after 150 ns, of DynA peptide interacting with pure DMPC (left) and DMPC/Chol (right) membranes. The DMPC/Chol snapshot was taken from the DMPC/Chol 2 simulation. DynA is in space-fill, and the membrane shape can be traced from the positions of phosphate atoms (depicted in gold) on the two membrane leaflets. For clarity, the remaining lipid atoms as well as the salt atoms are removed. The water atoms surrounding membranes are shown in red. The bilayer normal z axis is drawn to highlight the location of the bilayer midplane ($z = 0$), and yellow lines are guides that illustrate different extents of DynA tilting in DMPC and DMPC/Chol membranes.

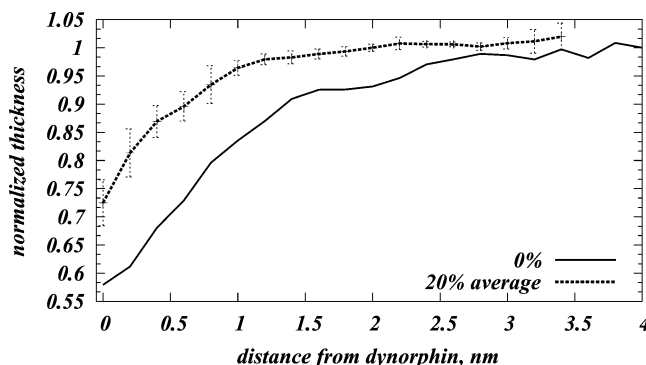


Figure 6. Deformation of the model membranes around DynA. Bilayer thickness (d_{HH}), normalized by its value far from the insertion, is plotted as a function of radial distance from DynA for all the simulated systems. For cholesterol-containing bilayers, the profile is the average over three independent calculations, and the error bars indicate standard deviations calculated from the three DMPC/Chol simulations. For this analysis, the simulated box around the insertion was divided into radial slices with $dr = 2 \text{ \AA}$, and the histogram was constructed of phosphate-to-phosphate distance in each bin, and for all the frames of the converged trajectory (70–150 ns). Final profiles were obtained by proper normalization of the events in each bin of the histogram.

(the profile for the DMPC/Chol is the average over the three independent simulations). Both the DMPC and DMPC/Chol systems are seen to deform around DynA, with the pure DMPC membrane showing a greater extent of thinning around the insertion (see also Figure 3B–E); note that the “unperturbed” bilayer is thicker in the DMPC/Chol system. The lipids in both systems reorganize as DynA equilibrates inside the membranes to minimize the level of hydrophobic mismatch between the natural bulk thickness of lipid membranes and the length of TM insertion^{41–44} (see below).

The radially varying d_{HH} profile is directly related to spatially nonuniform packing of lipid tails within the bilayers. This is illustrated in Figure 7 where the deuterium order parameters ($-S_{\text{CD}}$) are shown for DMPC lipid chains within a 10 Å radius shell around DynA (near) and outside this shell (far) for all the

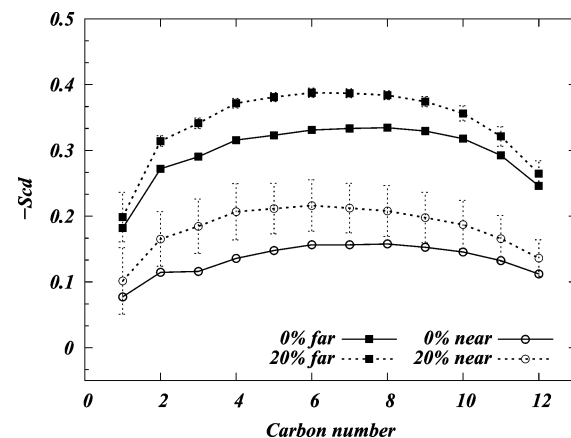


Figure 7. Lipid tail deuterium order parameters ($-S_{\text{CD}}$) for DMPC molecules that are within a 10 Å radial shell around DynA (near) and outside this area (far) for all the model systems. Profiles for DMPC/Chol mixtures are shown as averages over the three simulations, with error bars showing the standard deviations from the three DMPC/Chol trajectories. Note that the error bars in the “20% far” graph for the majority of the CH_2 groups are comparable to the symbol size used to plot this graph and thus are hardly visible.

model systems; $-S_{\text{CD}}$ at each methylene carbon atom along lipid tails is defined as

$$-S_{\text{CD}} = \left\langle \frac{1}{2}(3 \cos^2 \phi - 1) \right\rangle \quad (2)$$

where ϕ is the angle between the C–H bond vector and the bilayer normal and the angular brackets indicate averaging over time and over all the lipids. Consistent with variations in peak-to-peak distances in Figures 3 and 6, lower ordering is seen in Figure 7 for the lipids that are near the DynA, as compared to those far away in all the simulated systems. Overall, the DMPC acyl chains are more ordered in DMPC/Chol, in agreement with our electron density calculations in Figure 3A–E, as well as

with experimental^{67,73–78} and other computational^{33,79,80,82–85} studies on PC/Chol mixtures.

The observed membrane thinning near the insertion is accompanied by significant water penetration inside the bilayer hydrophobic core, as can be seen from Figure 5, as well as from the water electron density profiles in Figure 3F,G. That the presence of the TM peptide facilitates water partitioning has been described in theoretical and experimental studies of various bilayer-penetrating ligands (see, for instance, refs 39, 40, and 86–89 and references therein), as well as for TM segments of the 5HT_{2A} receptor.⁹⁰ From Figures 3F,G and 5, we find that the water density around the insertion is *not* uniform, in agreement with earlier MD studies of DynA in pure DMPC membranes.^{39,40} Thus, more waters are present near the DynA polar residues, as well as around residues at the N-terminus of DynA (see Figure 3F,G). These waters follow the lipid headgroups from the bottom (DynA-free) leaflet (Figure 5), and thus penetrate deep into the membrane core. Not surprisingly, we find the N-terminus of the DynA peptide to be partially protonated in our simulations. Thus, the pK_a value of the amine group in pure DMPC membrane is ~7.9, estimated following Mehler and Guarneri,⁹¹ even though the peptide is immersed into the hydrophobic core of the bilayer. The estimated pK_a is higher than would be expected for a fully buried amine group because the amine group in the DMPC membrane interacts strongly with the solvent, lipid backbone, and headgroup atoms on the opposite bilayer leaflet, since the membrane thins around the peptide, as illustrated in Figure 5 where the amine group of the DynA is surrounded by the phosphate atoms.

The main findings of our work, that identify essential elements in the effects of cholesterol, are (i) that DynA is located higher, toward the lipid/water interface, and in a more vertical orientation in DMPC/Chol than in DMPC bilayers; and (ii) the greater thinning of DMPC membranes around the peptide, and stronger water influx, compared to that observed in the DMPC/Chol. To obtain a quantitative measure for the determinants of these key observations, we undertook a quantitative analysis of DynA-induced membrane deformations using the continuum theory of membrane deformations (CTMD) which is based on hydrophobic mismatch as described in Methods. This analysis is detailed below and shows that it is necessary to correct the CTMD approach to account for the lipid packing energy contribution. The implications of these results for the function of κ-opioid receptors that bind DynA, and the possible involvement of lipid rafts, are then discussed.

Mechanism of Regulation of DynA Dynamics and Membrane Response by Cholesterol. Our finding that DynA is closer to the lipid headgroups and in a more vertical orientation in DMPC/Chol membranes compared to pure DMPC bilayer is reminiscent of previous descriptions of the role of cholesterol in the membrane organization of various antimicrobial peptides (see refs 92–96 and references therein). It reflects cholesterol's ability to influence the organization and dynamics of TM insertions by imposing aligning force on the insertions. In particular, we have recently demonstrated³³ that the orientation and vertical location of cholesterol itself in DMPC bilayers is determined by the aligning field from other cholesterol molecules, and we have developed a mechanistic picture of how this field may affect the dynamics of the inserted Dyna.

When the Chol concentration increases from 1 to 40%, cholesterol molecules undergo a transition from a “lying down” to a “standing up” orientation, whereby the Chol tilt with respect to the bilayer normal is reduced and the hydroxyl group of the cholesterol moves closer to the lipid/water interface.³³ This is

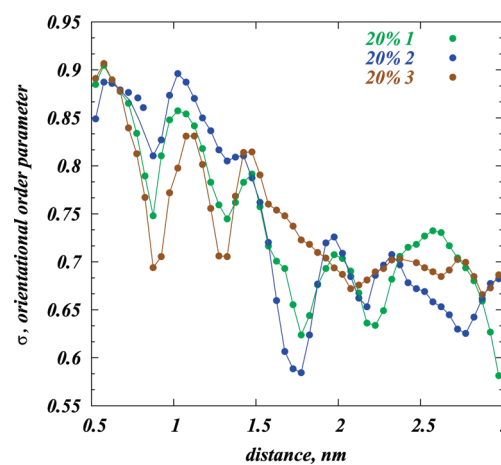


Figure 8. Cholesterol orientational order parameter σ (see text) as a function of distance between cholesterols. The results for three DMPC/Chol simulations are shown as colored dots, and the lines connect the data points.

because, at high cholesterol content, enthalpic interactions between Chol–Chol and Chol–lipid become stronger than the orientational entropy of cholesterol molecules.³³ The latter, however, dominates the free energy at low cholesterol concentrations.³³

A long-range order is observed around 20% Chol, where Chols tend to align along the bilayer normal. As a consequence, the material properties of phospholipid membranes change with increasing Chol concentration, as cholesterol-rich bilayers show greater rigidity compared to low-Chol membranes.³⁴

To discuss this aligning field and its role in organization of DynA, we define cholesterol's orientational order parameter σ ^{33,97} as

$$\sigma = \left\langle \frac{1}{2}(3 \cos^2 \alpha - 1) \right\rangle \quad (3)$$

where α denotes the angle between the ring planes of two cholesterol and the angular brackets indicate averaging over time and over all the Chol–Chol pairs. Thus, $\sigma = 1$ if Chol molecules are perfectly aligned and $\sigma = 0$ for the orientationally isotropic mixture.⁹⁷ In Figure 8, we show the calculated σ as a function of the distance between cholesterol pairs for the 20% mixtures. The existence of the aligning field inside the bilayers is evident from the high σ values even for Chol–Chol pairs that are largely separated, suggesting that the orientational ordering of Chol molecules in these bilayers persists over large distances. Note also that σ curves show periodicities in r , suggesting that neighboring Chol molecules tend to avoid direct contact with each other by separating themselves with DMPC lipid molecules.

The orientational entropy losses are given by³³

$$\Delta S = -k_B \int_0^{\pi/2} P(\theta) \log \left[\frac{P(\theta)}{\sin \theta} \right] d\theta \quad (4)$$

where $P(\theta)$ represents the normalized probability density of cholesterol tilt angle θ with respect to the bilayer normal (see Methods) and k_B is the Boltzmann constant. As defined above, the orientational entropy vanishes if Chol molecules are randomly oriented.³³ In DMPC/Chol, however, ΔS is expected to deviate from zero, due to the anisotropic orientation of

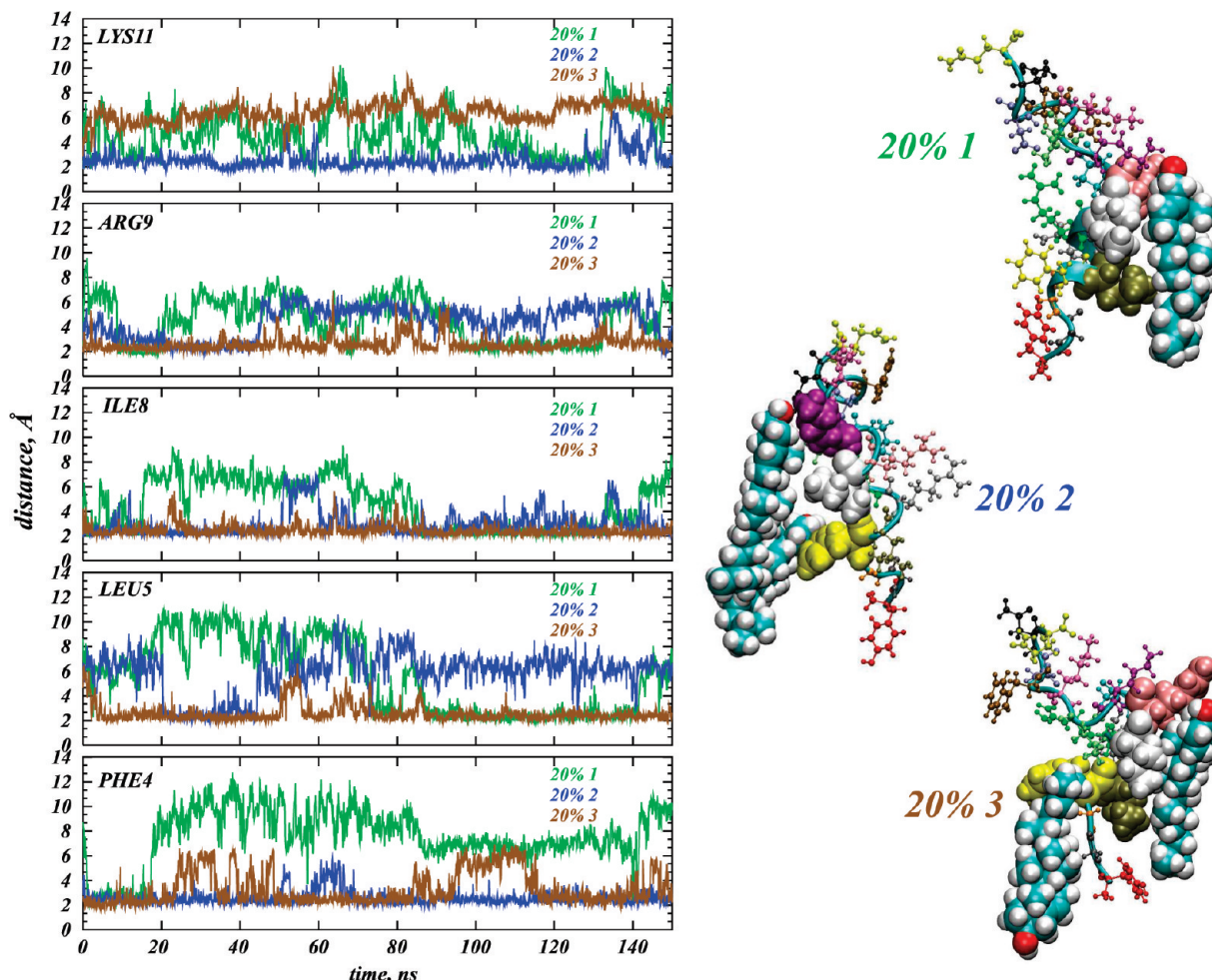


Figure 9. Cholesterol dynamics around selected residues on DynA. The panels show the time evolution of the minimum distance between cholesterol and Phe4, Leu5, Ile8, Arg9, and Lys11 residues in three DMPC/Chol simulations, and the cartoons depict representative snapshots from each simulation. In these snapshots, cholesterol is drawn in space-fill, and the different residues of DynA are drawn in various colors, using red for N-terminal Tyr1. The key DynA residues are highlighted in space-filled rendering utilizing the following shades: Phe4 - yellow, Leu5 - tan, Ile8 - white, Arg9 - pink, and Lys11 - purple.

cholesterol. Indeed, we calculate ΔS for our DMPC/Chol systems to be $-1.9 \pm 0.1 k_B$.

As the Chols align, they become engaged in interactions with neighboring DMPC lipids giving rise to cholesterol's so-called condensing effect on phospholipids,^{33–38} where the lipid hydrocarbon chains become more ordered (Figure 7), while the bilayer thickens (Figure 3A). Because this ordering effect is observed also for lipids in the vicinity of DynA (Figure 7), the aligning field resulting in cholesterol condensation must have an effect on the organization of DynA as well. In particular, the long-range orientational order that is established by Chols will keep DynA in a relatively straight orientation. As a result, charged residues on the DynA helix and at the C-terminus of the peptide will engage in strong hydrophilic interactions with the lipid headgroup and solvent atoms, due to the closeness of these residues to the lipid/water interface when the DynA is in the upright conformation. These favorable enthalpic contributions as well as the losses in the peptide orientational flexibility due to cholesterol condensation will limit DynA membrane penetration in DMPC/Chol systems.

We do not observe cholesterol enrichment around DynA. From the average mole fraction of cholesterol and DMPC within a 10 Å radial shell around DynA during the last 80 ns of the three DMPC/Chol simulations, we found the Chol mole fraction in the vicinity of the peptide to be in the range of 12 and 18%

within three simulations, i.e., lower than the bulk Chol composition. However, several DynA residues appear to be in contact with Chol molecules for extended periods of simulation time (Figure 9). The figure reveals that, in the third trajectory for the 20% system, a single cholesterol is involved in interactions with Phe4, whereas another Chol interacts simultaneously with Leu5, Ile8, and Arg9. In the second trajectory, one Chol interacts with Phe4, and another one is involved in interactions with Ile8 and Lys11, whereas, in trajectory 1, we identify a single cholesterol molecule interacting simultaneously with Leu5, Ile8, and Arg9 residues.

CTMD Captures the Membrane Deformations in DMPC but Not Those in DMPC/Chol Membranes. The DynA-induced membrane thinning observed in our simulations can be characterized quantitatively using the continuum theory of bilayer deformations, CTMD^{41–44} (see Methods). Figure 10 shows the results of the minimization procedure implemented for the CTMD (see Methods) to obtain equilibrium membrane shapes around DynA and the corresponding deformation free energies for our simulated DMPC and DMPC/Chol systems. As before, for the Chol-containing bilayers, the values from the MD simulations were averaged over the three different trajectories. Because in the DMPC/Chol simulations we observed a somewhat low fraction of cholesterol around the DynA compared to that in the “bulk” (see above), the CTMD procedure

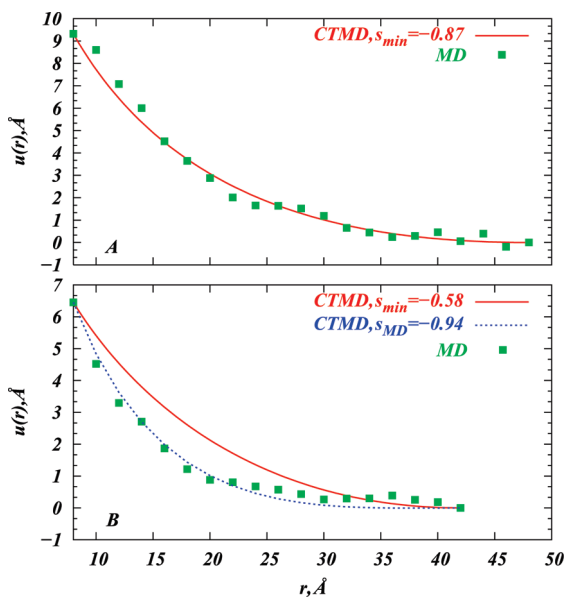


Figure 10. Comparison of DynA-induced membrane deformations obtained from MD simulations and continuum theory of membrane deformations (CTMD) for DMPC (A) and DMPC/Chol (B) bilayers. Profiles of membrane deformations $u(r)$ are shown as a function of distance from DynA in different simulated systems. For DMPC/Chol, the data are averaged over the three independent trajectories. The MD predictions are depicted as symbols, and equilibrium shapes from the self-consistent CTMD are plotted as solid lines. The solutions in both panels correspond to the values of packing parameter s_{\min} that minimize the free energy functional in eq 1. For the DMPC/Chol system, we also illustrate with a dashed line one alternative solution for $u(r)$ obtained from CTMD based on the value of the packing parameter obtained from the MD simulations. For calculations using the CTMD, the parameter set listed in Table 2 and r_0 was set to 8 Å as the average radius of the DynA helix derived from the MD simulations. Therefore, the DynA surface in these plots is located at $r = 8$ Å distance.

for the DMPC/Chol mixtures was conducted with both constant (taken from Table 2) and spatially varying bending and compressibility.⁹⁸ For the latter case, the values for K_c and K_a given in Table 2 were chosen to represent the moduli of the “bulk”, and K_c and K_a exponentially decayed to two-thirds of their bulk values inside the 10 Å radial region around the DynA. Because the two CTMD calculations, using the constant and the spatially varying moduli, resulted in the same equilibrium membrane deformations, in Figure 10B, we only show the CTMD solution (s_{\min}) corresponding to the constant elastic modulus.

Figure 10A reveals good agreement between the shape predicted by the MD simulations and the self-consistent solution of the CTMD; the DynA-induced equilibrium deformation energy in the DMPC membrane is calculated to be $6.84 k_B T$. In the DMPC/Chol simulations, however, we observe a discrepancy between the deformation profile deduced from the MD simulations and from the self-consistent CTMD analysis (Figure 10B). The difference is likely to stem from the contrasting estimates of the lipid tail packing parameter emerging from the two approaches, as the slopes of the two data sets in Figure 10B, representing solutions from the MD and from the CTMD corresponding to s_{\min} , are different. The deformation free energies for s_{\min} and s_{MD} solutions are $21.1 k_B T$ and $36.8 k_B T$, respectively.

Consequently, our finding that the CTMD reproduces the MD data for pure DMPC but not for DMPC/Chol can be explained by the different energy costs calculated by the two approaches for the tilt of hydrocarbon lipid tails in 0 and 20% Chol mixtures.

In particular, in DMPC/Chol systems, this energy cost should be expected to be substantial, due to the more liquid-ordered nature of these membranes. Indeed, a relatively low value for the empirical cholesterol tilt modulus, χ (see Methods), in DMPC/Chol membranes at various sterol compositions was estimated recently for mixtures containing less than 10% Chol.³³ However, a $7 k_B T/\text{rad}^2$ increase in χ occurs between 10 and 20% Chol, after which it remains relatively constant ($17 \pm 4 k_B T/\text{rad}^2$) as the cholesterol concentration increases further.³³ For the present simulations with 20% Chol, we also calculate χ to be substantial, $25 \pm 3 k_B T/\text{rad}^2$, suggesting that the energy related to tilting the Chol molecules in the 20% mixtures can be much larger than in low-Chol membranes. This conclusion confirms a well-known feature of raft-like membranes, the strong resistance to any deformation or lipid tilting.

This characteristic of Chol-containing membranes is not captured by the CTMD approach, which treats the lipid tail packing contribution only implicitly, through the packing parameter s .^{42,43} (see Methods). Although such treatment quantitatively captures insertion-induced deformations in membranes where the energy cost related to tilt of hydrocarbon lipid tails is small,^{42–44} our analysis suggests that, in bilayers where the lipid tilt energy is substantial, the CTMD framework needs to be complemented with an additional term describing the energy of lipid packing around the insertion.⁴² This is illustrated in Figure 10B, which shows a solution from the CTMD approach using the value of the packing parameter that we obtained from the MD trajectories of DMPC/Chol systems. There is excellent agreement with the MD solution, suggesting that it is possible to use MD simulations to capture the effect of lipid packing in the CTMD approach. Such an enhancement should improve the performance of this coarse-grained methodology for raft-like lipid mixtures and enable the CTMD (complemented by MD) to become a general tool for describing interactions between lipid rafts and associated proteins, such as the GPCRs, and their membrane-embedded ligands.

Implications for the Function of κ -Opioid Receptors (KORs) and Lipid Rafts. Our results suggest an explanation for the experimentally observed affinity of KORs toward lipid rafts.²⁴ Specifically, Xu and co-workers²⁴ found that KORs are localized and function in rafts, and comparison of the KOR activity in intact vs Chol-depleted cells suggested that cholesterol is involved in modulating ligand binding and signaling efficiency of KOR. Additional experimental and theoretical explorations have addressed the general problem of identifying specific GPCR binding pathways for ligands that partition into lipid membranes before inserting into their target receptors.^{30–32,45,99} These studies have suggested that the entry site for such ligands lies close to the lipid/water interface. For example, Paterlini et al.⁹⁹ predicted that dynorphin A^{1–10} (Dyn10), a shorter analogue of DynA with a truncated C-terminus, will bind KOR near the extracellular (EC) loop 2, with the Arg6, Arg7, and Ile8 residues of Dyn10 positioned within 5 Å of the Ser7.34-Tyr7.35-Tyr7.36-Phe7.37 sequence in the receptor (residue numbering according to the Ballesteros/Weinstein generic scheme¹⁰⁰), and with Glu6.58 in TM6 of KOR. Recently, Hurst et al.³⁰ have simulated the entry of the endogenous cannabinoid ligand *sn*-2-arachidonylglycerol (2-AG) into CB2 GPCR and predicted that 2-AG is embedded in the membrane when it engages in interactions with Phe7.35 and Cys7.38 of the CB2 receptor before proceeding to its binding site. Interestingly, Park et al.³² identified two distinct openings in the crystal structure of ligand-free opsin, involving residues Ile5.40 and Phe5.43 on TM5, Phe6.56, and

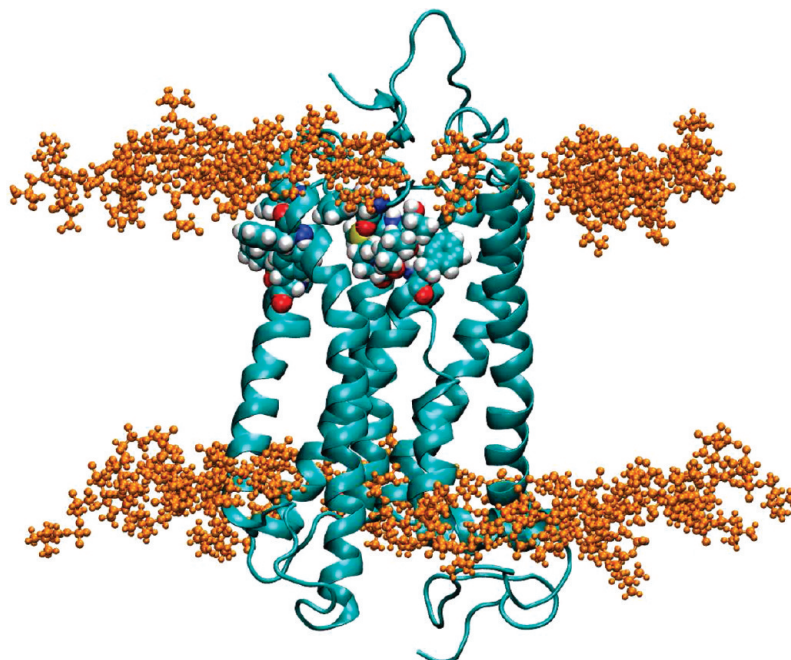


Figure 11. Snapshot from MD simulations of rhodopsin (PDB accession 1U19) in a mixed 1-stearoyl-2-docosahexaenyl-*sn*-glycero-3-phosphocholine (SDPC)/1-stearoyl-2-docosahexaenyl-*sn*-glycero-3-phosphoethanolamine (SDPE) lipid/cholesterol membrane, adopted from ref 27, highlighting in space-filling rendering the residues at locations 7.34, 7.35, 7.36, 7.37, 7.38, 7.40, 6.56, 6.59, 5.40, and 5.43. Rhodopsin is shown in cartoon, and lipid headgroup atoms are depicted in ball-and-stick representation. The rest of the membrane atoms as well as water and salt ions are removed for clarity.

Phe 6.59 on TM6, and Phe7.40 on TM7, that may serve as paths for the binding of retinal.

Taken together, these findings suggest that the pathways for bilayer-penetrating ligands to access their binding sites in the TM bundle may be located close to the lipid headgroup region. This is illustrated in Figure 11 which shows a snapshot from our recent MD simulations of rhodopsin (PDB accession 1U19) in 1-stearoyl-2-docosahexaenyl-*sn*-glycero-3-phosphocholine (SDPC)/1-stearoyl-2-docosahexaenyl-*sn*-glycero-3-phosphoethanolamine (SDPE)/cholesterol lipid membrane,²⁷ the rhodopsin residues that correspond to those mentioned above for cognate GPCRs are highlighted.

In order to compare the DynA positions in our DMPC and DMPC/Chol membranes with the locations of the key residues in Figure 11, we calculated the vertical displacement (along the bilayer normal) of each residue on DynA relative to a plane representing the average density of DMPC lipid backbone C2 carbon atoms, and compared these distances to the vertical positioning of the key GPCR residues in Figure 11 with respect to the same C2 atom density plane (in SDPC/SDPE/cholesterol bilayers) in the earlier rhodopsin simulations.²⁷ Overall, the organization of DynA in the DMPC/Chol membranes is such that residues 10–17 all reside within 3 Å of the C2 atoms, whereas in the pure DMPC system only residues 15–17 are found to be within the same range of the backbone carbons. For example, the Ile8–Arg9 pair of DynA is located at ~10 and ~5 Å within the hydrocarbon core in 0 and 20% DMPC/Chol mixtures, respectively. All the key residues depicted in Figure 11, and specifically the 7.34–7.37 sequence identified by Paterlini et al.⁹⁹ in relation to Dyn10–KOR interactions (see above), are within 5 Å of C2 atoms on SDPC and SDPE lipids in the simulations of rhodopsin.

Our analysis shows that the locations of the residues implicated in interactions with bilayer-penetrating GPCR ligands correlate better with the DynA positioning in DMPC/Chol than in DMPC. This suggests that cholesterol creates favorable

conditions for DynA to be positioned near the critical residues of the target GPCR, thereby facilitating the entry of DynA into the TM bundle of the KOR. Our predictions thus offer plausible mechanistics for KOR localization and enhanced function in cholesterol-enriched rafts.

The conclusions reached from our analysis for the DynA behavior in the cholesterol-containing membranes should be generalizable to other classes of ligands targeting their receptors through the membrane, including those of various subtypes of opioid and cannabinoid GPCRs. The extension to opioid peptides follows from the fact that, like DynA, other endogenous ligands also have significant helical stretches expected to behave in a similar fashion in response to increasing Chol concentrations.

While the cannabinoid ligands vary structurally, from unsaturated hydrocarbon chains (2-AG) to more rigid ring structures (AM-841) (see ref 30 and references therein), condensation of cholesterol on lipid membrane and the orientational aligning field discussed above will also affect the organization of these compounds in the membrane. In fact, studies have shown that Chol-enriched lipid rafts play a role in cannabinoid receptor function.¹⁰⁴ The similarity of the lipid-based binding pathways proposed for both cannabinoid and opioid ligands³⁰ (see Figure 11) suggests that cholesterol will play a similar role in regulating the entry of cannabinoid ligands into their target GPCRs.

Concluding Remarks

We have explored the role of cholesterol in the organization and dynamics of a prototypical ligand of the KOR GPCR that reaches its target from the membrane bilayer. From MD simulations of the DynA peptide in DMPC and DMPC/Chol model membranes, we found that DynA equilibrates with its N-terminal helix ~5 Å deeper into the lipid hydrocarbon core and in a more tilted orientation, with respect to the membrane normal, in pure DMPC bilayers than in DMPC/Chol mixtures. Concomitantly, the DMPC membrane shows more thinning

around the insertion and a larger water influx into the hydrophobic core than we found for DMPC/Chol.

The energy cost of the DynA-induced membrane deformations observed in our simulations was quantified with the application of CTMD-based methodology. Comparing the CTMD predictions to results from the corresponding MD simulations revealed the significance of a correct representation of the lipid tail packing energy contribution, and indicated a way in which the CTMD methodology could be refined to enable quantitative prediction for the equilibrium shape of raft-like lipid mixtures around TM insertions. With that, we lay a foundation for extending the applicability of the CTMD framework to lipid rafts and their interactions with membrane proteins and peptides, including GPCRs.

A mechanistic picture of cholesterol regulating organization and dynamics of bilayer-penetrating GPCR ligands emerges from our results. The specific application to DynA and its target GPCR provides as well an explanation for the experimental results suggesting preferred localization and better function of KOR in cholesterol-enriched rafts.²⁴ Specifically, our data show that cholesterol creates conditions that allow membrane-penetrating ligands to position near the residues on the target GPCR involved in the ligand entry pathways. With that, cholesterol may facilitate insertion of bilayer-binding ligands, such as DynA, into designated receptors.

Acknowledgment. We would like to thank Daniel Harries for insightful discussions and Ernest Mehler for the help setting up pKa calculations. The work is supported by grants from the National Institutes of Health P01 DA012408 and P01 DA012923. The molecular dynamics simulations were conducted on Tera-Grid computers (allocation MCB090132). Computational resources of the David A. Cofrin Center for Biomedical Information in the HRH Prince Alwaleed Bin Talal Bin Abdulaziz Alsaud Institute for Computational Biomedicine are also gratefully acknowledged.

References and Notes

- (1) Chini, B.; Parenti, M. *J. Mol. Endocrinol.* **2004**, *32*, 325.
- (2) Pike, L. J. *J. Lipid Res.* **2003**, *44*, 655.
- (3) Visiers, I.; Ballesteros, J. A.; Weinstein, H. *Methods Enzymol.* **2002**, *343*, 329.
- (4) Kobilka, B. K. *Biochim. Biophys. Acta* **2007**, *1768*, 794.
- (5) Kobilka, B. K.; Deupi, X. *Trends Pharmacol. Sci.* **2007**, *28*, 397.
- (6) Hubbell, W. L.; Altenbach, C.; Hubbell, C. M.; Khorana, H. G. *Adv. Protein Chem.* **2003**, *63*, 243.
- (7) Bartfai, T.; Benovic, J.; Bockaert, J.; Bond, R. A.; Bouvier, M.; Christopoulos, A.; Civelli, O.; Devi, L. A.; George, S. R.; Inui, A.; Kobilka, B. K.; Leurs, R.; Neubig, R.; Pin, J. P.; Quirion, R.; Roques, B. P.; Sakmar, T. P.; Seifert, R.; Stenkamp, R. E.; Strange, P. G. *Nat. Rev. Drug. Discovery* **2004**, *3*, 577.
- (8) Kristiansen, K. *Pharmacol. Ther.* **2004**, *103*, 21.
- (9) Filizola, M.; Weinstein, H. *Curr. Opin. Drug. Discovery Dev.* **2005**, *8*, 577.
- (10) Pucadyil, T. J.; Chattapadhyay, A. *Prog. Lipid Res.* **2006**, *45*, 295.
- (11) Burger, K.; Gimpl, G.; Fahrenholz, F. *Cell. Mol. Life Sci.* **2000**, *57*, 1577.
- (12) Lingwood, D.; Simons, K. *Science* **2010**, *327*, 46.
- (13) McMullen, T. P. W.; Lewis, R. N. A. H.; McElhaney, R. N. *Curr. Opin. Colloid Interface Sci.* **2004**, *8*, 459.
- (14) Lichtenber, D.; Goni, F. M.; Heerklotz, H. *Trends Biochem. Sci.* **2005**, *30*, 430.
- (15) Khelashvili, G.; Scott, H. L. *J. Chem. Phys.* **2004**, *120*, 9841.
- (16) Simons, K.; Ikonen, E. *Nature* **1997**, *387*, 569.
- (17) Brown, D. A. *Physiology* **2006**, *21*, 430.
- (18) Veatch, S. L.; Keller, S. L. *Biochim. Biophys. Acta* **2005**, *1746*, 172.
- (19) Edidin, M. *Annu. Rev. Biophys. Biomol. Struct.* **2003**, *32*, 257.
- (20) Munro, S. *Cell* **2003**, *115*, 377.
- (21) Simons, K.; Vaz, W. L. *Annu. Rev. Biophys. Biomol. Struct.* **2004**, *33*, 269.
- (22) Varma, R.; Mayor, S. *Nature* **1998**, *394*, 798.
- (23) Friedrichson, T.; Kurzhalia, T. V. *Nature* **1998**, *394*, 801.
- (24) Xu, W.; Yoon, S.-I.; Huang, P.; Wang, Y.; Chen, C.; Chong, P. L.-G.; Chen, L.-Y. L. *J. Pharmacol. Exp. Ther.* **2006**, *317*, 1295.
- (25) Boesze-Battaglia, K.; Hennessey, T.; Albert, A. D. *J. Biol. Chem.* **1989**, *264*, 8151.
- (26) Weinstein, H. *AAPS J.* **2006**; E871.
- (27) Khelashvili, G.; Grossfield, A.; Feller, S. E.; Pitman, M. C.; Weinstein, H. *Proteins: Struct., Funct., Bioinf.* **2009**, *76*, 403.
- (28) Schwyzer, R. *Biopolymers* **1991**, *31*, 785.
- (29) Schwyzer, R. *Biopolym. Pept. Sci.* **1995**, *37*, 5.
- (30) Hurst, D. P.; Grossfield, A.; Lynch, D. L.; Feller, S.; Romo, T. D.; Gawrisch, K.; Pitman, M. C.; Reggio, P. H. *J. Biol. Chem.* **2010**, *285*, 17954.
- (31) Pei, Y.; Mercier, R. W.; Anday, J. K.; Thakur, G. A.; Zvonok, A. M.; Hurst, D.; Reggio, P. H.; Janero, D. R.; Makriyannis, A. *Chem. Biol.* **2008**, *15*, 1207.
- (32) Park, J. H.; Scheerer, P.; Hofmann, K. P.; Choe, H. W.; Ernst, O. P. *Nature* **2008**, *454*, 183.
- (33) Khelashvili, G.; Pabst, G.; Harries, D. *J. Phys. Chem. B* **2010**, *114*, 7524.
- (34) Pan, J.; Mills, T. T.; Tristam-Nagle, S.; Nagle, J. F. *Phys. Rev. Lett.* **2008**, *100*, 198103.
- (35) Hodzic, A.; Rappolt, M.; Amenitsch, H.; Laggner, P.; Pabst, G. *Biophys. J.* **2008**, *94*, 3935.
- (36) Meyer, F. de; Smit, B. *Proc. Natl. Acad. Sci. U.S.A.* **2009**, *106* (10), 3654.
- (37) Greenwood, A. I.; Tristam-Nagle, S.; Nagle, J. F. *Chem. Phys. Lipids* **2006**, *143*, 1.
- (38) Hung, W. C.; Lee, M. T.; Chen, F. Y.; Huang, H. W. *Biophys. J.* **2007**, *92*, 3960.
- (39) Sankararamakrishnan, R.; Weinstein, H. *Biophys. J.* **2000**, *79*, 2331.
- (40) Sankararamakrishnan, R.; Weinstein, H. *J. Phys. Chem. B* **2002**, *106*, 209.
- (41) Andersen, O. S.; Koeppe, R. E., II. *Annu. Rev. Biophys. Biomol. Struct.* **2007**, *36*, 107–130.
- (42) Nielsen, C.; Goulian, M.; Andersen, O. S. *Biophys. J.* **1998**, *74*, 1966.
- (43) Nielsen, C.; Andersen, O. S. *Biophys. J.* **2000**, *79*, 2583.
- (44) Lundbaek, J. A.; Werge, T.; Andersen, O. S.; Nielsen, C. *Biophys. J.* **2003**, *84*, 2080.
- (45) Hildebrand, P. W.; Scheerer, P.; Park, J. H.; Choe, H. W.; Piechnick, R.; Ernst, O. P.; Hofmann, K. P.; Neck, M. *PLoS One* **2009**, *4*, e4382.
- (46) Uezono, T.; Toraya, S.; Obata, M.; Nishimura, K.; Tuzi, S.; Saitô, H.; Naito, A. *J. Mol. Struct.* **2005**, *749*, 13.
- (47) Ramamoorthy, A.; Lee, D.-K.; Narasimhaswamy, T.; Nanga, R. P. R. *Biochim. Biophys. Acta* **2010**, *1798*, 223–227.
- (48) Almeida, P. F. F.; Vaz, W. L. C.; Thompson, T. E. *Biochemistry* **1992**, *31*, 6739.
- (49) Tessmer, M. R.; Kallick, D. A. *Biochemistry* **1997**, *36*, 1971.
- (50) Jo, S.; Lim, J. B.; Klauda, J. B.; Im, W. *Biophys. J.* **2009**, *97*, 50.
- (51) MacKerell, A. D., Jr.; Bashford, D.; Bellot, M.; Dunbrack, R., Jr.; Evanseck, J.; Field, M.; Fischer, S.; Gao, J.; Guo, H.; Ha, S.; Joseph McCarthy, D.; Kuchnir, L.; Kuczera, K.; Lau, F.; Mattos, C.; Michnick, S.; Ngo, T.; Nguyen, D.; Prodhom, B.; Reiher III, W.; Roux, B.; Schlenkrich, M.; Smith, J.; Stote, R.; Straub, J.; Watanabe, M.; Wiorkiewicz-Kuczera, J.; Yin, D.; Karplus, M. *J. Phys. Chem. B* **1998**, *102*, 3586.
- (52) Klauda, J. B.; Brooks, B. R.; MacKerell, A. D., Jr.; Venable, R. M.; Pastor, R. W. *J. Phys. Chem. B* **2005**, *109*, 5300.
- (53) Feller, S. E.; Gawrisch, K.; MacKerell, A. D., Jr. *J. Am. Chem. Soc.* **2002**, *124*, 318.
- (54) Pitman, M.; Suits, F.; MacKerell, A. D., Jr.; Feller, S. E. *Biochemistry* **2002**, *43*, 15318.
- (55) Phillips, J. C.; Braun, R.; Wang, W.; Gumbart, J.; Tajkhorshid, E.; Villa, E.; Chipot, C.; Skeel, R. D.; Kale, L.; Schulten, K. *J. Comput. Chem.* **2005**, *26*, 1781.
- (56) Essmann, U.; Perera, L.; Berkowitz, M. L.; Darden, T.; Lee, H.; Pedersen, L. G. *J. Chem. Phys.* **1995**, *103*, 8577.
- (57) Martyna, G. J.; Tobias, D. J.; Klein, M. L. *J. Chem. Phys.* **1994**, *101*, 4177.
- (58) Feller, S. E.; Zhang, Y.; Pastor, R. W.; Brooks, B. R. *J. Chem. Phys.* **1995**, *103*, 4613.
- (59) Mezei, M.; Filizola, M. *J. Comput.-Aided Mol. Des.* **2006**, *20*, 97.
- (60) Kabsch, W.; Sander, C. *Biopolymers* **1983**, *22*, 2577.
- (61) Helfrich, W. *Z. Naturforsch.* **1973**, *28c*, 693.
- (62) Andelman, D.; Kozlov, M. M.; Helfrich, W. *Europhys. Lett.* **1994**, *25*, 231.
- (63) Khelashvili, G.; Harries, D.; Weinstein, H. *Biophys. J.* **2009**, *97*, 1626.
- (64) Zimmerberg, J.; Kozlov, M. M. *Nat. Rev. Mol. Cell Biol.* **2006**, *7*, 9.
- (65) Chen, Z.; Rand, R. P. *Biophys. J.* **1997**, *73*, 267.

- (66) Kessel, A.; Ben-Tal, N.; May, S. *Biophys. J.* **2001**, *81*, 643.
(67) Pan, J.; Mills, T. T.; Tristam-Nagle, S.; Nagle, J. F. *Phys. Rev. Lett.* **2008**, *100*, 198103.
(68) Rappolt, M.; Vidal, M. F.; Kriechbaum, M.; Steinhart, M.; Amentisch, H.; Bernstorff, S.; Laggner, P. *Eur. Biophys. J.* **2003**, *31*, 575.
(69) Gallova, J.; Uhrikova, D.; Hanulova, J.; Teixeria, J.; Balgavy, P. *Colloids Surf., B* **2004**, *38*, 11.
(70) McIntosh, T. J. *Biochim. Biophys. Acta* **1978**, *513*, 43.
(71) Hodzic, A.; Rappolt, M.; Amentisch, H.; Laggner, P.; Pabst, G. *Biophys. J.* **2008**, *94*, 3935.
(72) Tulenko, T. N.; Chen, M.; Mason, P. E.; Mason, R. P. *J. Lipid Res.* **1998**, *39*, 947.
(73) Douliez, J.-P.; Léonard, A.; Dufourc, E. J. *J. Phys. Chem.* **1996**, *100*, 18450.
(74) Urbina, J. A.; Peterar, S.; Le, H.-B.; Patterson, J.; Montez, B.; Oldfield, E. *Biochim. Biophys. Acta* **1995**, *1238*, 163.
(75) Urbina, J. A.; Moreno, B.; Arnold, W.; Taron, C. H.; Orlean, P.; Oldfield, E. *Biophys. J.* **1998**, *75*, 1372.
(76) Nielsen, M.; Thewalt, J.; Miao, L.; Ipsen, J. H.; Bloom, M.; Zuckermann, M. J.; Mouritsen, O. G. *Europhys. Lett.* **2000**, *52*, 368.
(77) Sankaram, M. B.; Thompson, T. E. *Biochemistry* **1990**, *29*, 10676.
(78) Marsan, M. P.; Muller, I.; Ramos, C.; Rodriguez, F.; Dufoure, E. J.; Czaplicki, J.; Milon, A. *Biophys. J.* **1999**, *76*, 351.
(79) Pasenkiewicz-Gierula, M.; Rög, T.; Kitamura, K.; Kusumi, A. *Biophys. J.* **2000**, *78*, 1376.
(80) Rög, T. Pasenkiewicz-Gierula, M. Vattulainen, I. Karttunen, M. *Biochim. Biophys. Acta* **2009**, *1788*, 97–121.
(81) Aitttoniemi, J.; Rög, T.; Pasenkiewicz-Gierula, M.; Karttunen, M.; Vattulainen, I. *J. Phys. Chem. B* **2006**, *110*, 25562.
(82) Smolyrev, A. M.; Berkowitz, M. L. *Biophys. J.* **2001**, *80*, 1649.
(83) Czub, J.; Baginski, M. *Biophys. J.* **2006**, *90*, 2368.
(84) Rög, T.; Pasenkiewicz-Gierula, M. *Biophys. Chem.* **2004**, *107*, 151.
(85) Jedlovsky, P.; Mezei, M. *J. Phys. Chem. B* **2003**, *107*, 5311.
- (86) Bachar, M.; Baker, O. *J. Chem. Phys.* **1999**, *111*, 8672.
(87) Li, S.; Su, Y.; Luo, W.; Hong, M. *J. Phys. Chem. B* **2010**, *114*, 4063.
(88) Sevcik, E.; Pabst, G.; Jilek, A.; Lohner, K. *Biochim. Biophys. Acta* **2007**, *1768*, 2586.
(89) Huang, H. W. *Biochim. Biophys. Acta* **2006**, *1758*, 1292.
(90) Duong, T. H.; Mehler, E. L.; Weinstein, H. *J. Comput. Phys.* **1999**, *151*, 358.
(91) Mehler, E. L.; Guarneri, F. *Biophys. J.* **1999**, *77*, 3.
(92) Thennarasu, S.; Tan, A.; Penumatchu, R.; Shelburne, C. E.; Heyl, D. L.; Ramamoorthy, A. *Biophys. J.* **2010**, *98*, 248.
(93) Hallock, K. J.; Lee, D.-K.; Omnaas, J.; Mosberg, H. I.; Ramamoorthy, A. *Biophys. J.* **2002**, *83*, 1004.
(94) Sooda, R.; Kinnunen, P. K. J. *Biochim. Biophys. Acta* **2008**, *1778*, 1460.
(95) Wessman, P.; Strömstedt, A. A.; Malmsten, M.; Edwards, K. *Biophys. J.* **2008**, *95*, 4324.
(96) Kin, T.; Im, W. *Biophys. J.* **2010**, *99*, 175.
(97) Kramer, D.; Ben-Shaul, A.; Chen, Z.-Y.; Gelbart, W. M. *J. Chem. Phys.* **1992**, *96*, 2236.
(98) Partenskii, M. B.; Jordan, P. C. *J. Chem. Phys.* **2002**, *117*, 10768.
(99) Paterlini, G. P.; Portoghesi, P. S.; Ferguson, D. M. *J. Med. Chem.* **1997**, *40*, 3254.
(100) Ballesteros, J. A.; Weinstein, H. *Methods Neurosci.* **1995**, *25*, 366.
(101) Elliott, J. R.; Haydon, D. A. *Biochim. Biophys. Acta* **1979**, *557*, 259.
(102) Needham, D. D.; McIntosh, T. J.; Evans, E. *Biochemistry* **1988**, *27*, 4668.
(103) Evans, E.; Rawicz, W. *Phys. Rev. Lett.* **1990**, *64*, 2094.
(104) Bari, M.; Battista, N.; Fezza, F.; Finazzi-Agro, A.; Maccarrone, M. *J. Biol. Chem.* **2005**, *280*, 12212.

JP106373R